

Solar Models with Helioseismic Constraints and the Solar Neutrino Problem

Satoru WATANABE and Hiromoto SHIBAHASHI

Department of Astronomy, School of Science, The University of Tokyo, Bunkyo-ku, Tokyo 113-0033
watanabe@astron.s.u-tokyo.ac.jp

(Received 2000 December 28; accepted 2001 April 25)

Abstract

Imposing a constraint of the sound-speed profile determined from helioseismology and updating the microphysics, we have revised our seismic solar model, constructed with the assumption of a homogeneous metal abundance distribution, and have shown that the theoretically expected neutrino fluxes are still significantly more than the observations. With the same sound-speed profile constraint, we also constructed solar models with low metal abundance in the core, and evaluated the neutrino fluxes of these models to see if nonstandard solar models with a low metal core can solve the solar neutrino problem. Some of these models are in agreement with the Homestake data, the Super-Kamiokande data, and the sound-speed profile simultaneously, but none of these satisfy both the neutrino flux data, including GALLEX and SAGE, and the helioseismically determined density profile.

Key words: neutrinos — Sun: abundances — Sun: helioseismology — Sun: interior — Sun: oscillations

1. Introduction

Various nonstandard solar models have been proposed to explain the deficit of neutrino fluxes from the Sun compared with the theoretical expectation based on the standard evolutionary models of the Sun. Solar models having a core with low heavy element abundance, Z , are such examples (Joss 1974; Levy, Ruzmaikina 1994; Jeffery et al. 1997). It is expected that a low Z in the central region of the Sun would lead to low opacity there, resulting in a lower central temperature; such models are expected to be in better agreement with the observed neutrino fluxes. However, nonstandard solar models have often been criticized: either their properties are in substantial disagreement with seismic data, or their sound-speed profile disagrees significantly with the seismically determined sound-speed profile of the Sun (e.g. Bahcall et al. 1997; Gough 1999). For example, comparing the observed data and the model predictions of the frequency difference between the n -th overtone p-mode of the low-degree l and the $(n-1)$ -th overtone p-mode of the degree $l+2$, which is sensitive to the structure of the solar central region, Guenther and Demarque (1997) claimed that low- Z cores extending beyond $0.06M_{\odot}$ should be ruled out because, otherwise, the model predictions would be in disagreement with the observed data and, furthermore, there would be no chance that the low- Z core models could reduce the neutrino capture rates below ~ 4.87 SNU and ~ 119 SNU for the Homestake neutrino detector using ^{37}Cl and the GALLEX and SAGE detectors using ^{137}Ga , respectively, while the detected capture rates are $\sim 2.56 \pm 0.23$ SNU and $\sim 72 \pm 8$ SNU, respectively (A SNU is defined to be 10^{-36} interactions s^{-1} per target atom). Such criticisms are, however, not necessarily fair, because those models

were constructed without fine tuning to agree with the helioseismic data.

The recent observations of solar oscillations provide us with a large number of very accurate eigenfrequencies of the Sun. The relative errors in the frequency measurement are as small as 10^{-6} . With the inversion of these frequencies, we now know the sound-speed profile in the Sun, $c(r)$, within errors of a few tenths of a percent. Imposing the constraint of the thus-obtained sound-speed profile, the profiles of temperature, density, pressure, luminosity, and chemical composition can be deduced (Shibahashi 1993; Shibahashi, Takata 1996).

It should be stressed here that the sound-speed profile has been very precisely determined from helioseismology, and that the difference between the profile determined in this way and that of any standard evolutionary solar model is demonstrably larger than the observational error. This means that we can also determine the profiles of thermal quantities in the Sun by using the observationally based highly accurate profiles for the acoustic quantities and adopting the same information of the microphysics (equation of state, nuclear reaction rates, and opacity) as used in constructing standard evolutionary solar models. The benefits of building such a solar model are as follows (Shibahashi 1993, 1999; Takata, Shibahashi 1998a, hereafter TS98a):

- We can construct a model of the present-day Sun without any assumption about the evolutionary history of the Sun. For example, we need not worry whether the ^3He induced g-mode instability and/or mass loss affects the evolution of the Sun.
- The location of the base of the convection zone, r_{conv} , can be estimated from the fact that the sound-

speed profile changes rapidly there (Gough 1984). Knowing the depth of the convection zone allows us to treat the radiative core only without worrying about the treatment of convection, which is not well-described theoretically (TS98a).

- The model is naturally consistent with the helioseismically determined sound-speed profile, while the evolutionary solar models are not necessarily so.

The main aim of this paper is to discuss our construction of solar models with an assumption of low Z in the core with the imposition of a constraint of the sound-speed profile, and to evaluate the neutrino fluxes of these models to see if nonstandard solar models with a low- Z core can solve the solar neutrino problem. Solar models based on helioseismology were constructed with an assumption that Z is homogeneous throughout the Sun (TS98a). Since then, the nuclear cross sections have been systematically recompiled and updated. Before discussing low- Z core models of the Sun, in section 3 we revise the seismic solar model with a homogeneous Z by adopting updated input physics. Then, in section 4, with the same input physics, we construct seismic solar models having a low- Z core and evaluate their neutrino fluxes. The preliminary results were presented at the SOHO-10/GONG-2000 joint workshop (Watanabe, Shibahashi 2000). We describe here our method in more detail, and present the latest results, including an estimate of the errors in the model properties and in the neutrino fluxes.

2. Equations of the Seismic Solar Model

We solve the basic equations governing the radiative core of the Sun with the imposition of information from helioseismology (TS98a, Takata, Shibahashi 1998b, hereafter TS98b, 1999; Shibahashi et al. 2000). They are the continuity equation,

$$\frac{dM_r}{dr} = 4\pi r^2 \rho, \quad (1)$$

the hydrostatic equation,

$$\frac{dP}{dr} = -\frac{GM_r \rho}{r^2}, \quad (2)$$

the energy equation,

$$\frac{dL_r}{dr} = 4\pi r^2 \rho \varepsilon, \quad (3)$$

and the energy transfer equation,

$$\frac{dT}{dr} = -\frac{3}{4ac} \frac{\kappa \rho}{T^3} \frac{L_r}{4\pi r^2}, \quad (4)$$

where the symbols have their usual meanings.

In addition to these differential equations, we need auxiliary equations: the equation of state, the equations for the opacity and the nuclear reaction rates:

$$\rho = \rho(P, T, X_i), \quad (5)$$

$$\kappa = \kappa(P, T, X_i), \quad (6)$$

and

$$\varepsilon = \varepsilon(P, T, X_i). \quad (7)$$

These equations link the thermal quantities and the chemical abundances. In making standard evolutionary models, the chemical abundance distribution is obtained by following the time evolution,

$$\frac{\partial X_i}{\partial t} = \left(\frac{\partial X_i}{\partial t} \right)_{\text{nuclear}} + \left(\frac{\partial X_i}{\partial t} \right)_{\text{diffusion}}, \quad (8)$$

where the nuclear reactions and the diffusion processes are taken into account. In the standard scenario, the chemical composition is assumed to be uniform at zero-age; $\partial X_i(t=0)/\partial r = 0$. In many nonstandard evolutionary models, some other time evolution processes are introduced and/or the initial conditions at $t=0$ are different from the standard case.

On the other hand, in constructing seismic models, we do not follow the time evolution. Instead, we impose the seismically determined sound-speed profile as a constraint on the model. Note that, if we distinguish only the hydrogen (^1H) and helium (^4He) separately as X and Y , respectively, and treat all other elements collectively as heavy elements, Z , then the sound-speed, as one of the thermodynamical quantities, is a function of two other thermodynamical quantities (P and T) and X and Z ,

$$c(P, T, X, Z) = c_{\text{obs}}(r). \quad (9)$$

This inversely relates the hydrogen abundance, X , with the pressure, temperature, metal abundance, and the sound-speed,

$$X = X(P, T, Z, c_{\text{obs}}). \quad (10)$$

Since X is given by equation (10) with the helioseismically determined sound-speed, the density, the opacity, and the nuclear reaction rate are, in turn, given in terms of $(P, T, Z, c_{\text{obs}})$ by equations (5)–(7).

If Z is given, then with the help of equation (10), the basic equations (1)–(4) can be solved with the proper boundary conditions. In principle, the helioseismically determined density profile, $\rho_{\text{obs}}(r)$, can be used as another constraint in constructing a seismic solar model. This constraint together with the sound-speed constraint determines the heavy elements' abundance profile, Z , at a given r as a part of the solution. Such attempts have indeed been carried out (TS98b). They have, however, not yet succeeded in obtaining a reasonable Z -profile in this way, since the dependence of the equation of state upon Z is so weak. We should also note that the formal error of $\rho_{\text{obs}}(r)$ is much larger than that of $c_{\text{obs}}(r)$. In this paper, therefore, we impose only the sound-speed profile as a constraint in constructing a seismic solar model, and we assume a certain Z -profile a priori.

In section 3, Z is assumed to be homogeneous for simplicity, following TS98a, while the microphysics is updated. In section 4, we assume that in the central core the heavy elements' abundance, Z , is lower than the outer part: low- Z core models. The schematic Z -profiles are shown in figure 1. A typical Z -profile of a standard evolutionary model with gravitational settling is shown in

figure 1 c (e.g., Bahcall et al. 1998, hereafter we refer to it as BP98). TS98b treated a rectilinear Z -profile and their Z -profile is just like figure 1 d.

The boundary conditions at the center are trivial:

$$M_r = 0 \quad \text{and} \quad L_r = 0 \quad \text{at} \quad r = 0. \quad (11)$$

The location of the base of the convection zone is estimated from the inverted sound-speed profile (Gough 1984). We adopt the seismically determined depth of the convection zone, $r = r_{\text{conv}}$, and set the outer boundary conditions at the base of the convection zone (TS98a):

$$\nabla_{\text{ad}} = \nabla_{\text{rad}} \equiv \frac{3\kappa L_r}{16\pi acGM_r T^4} \quad \text{and} \quad L_r = L_\odot \quad \text{at} \quad r = r_{\text{conv}}. \quad (12)$$

This means that we do not need to care about the convective heat transport, which has theoretical uncertainties. Moreover, chemical homogeneity in the convection zone requires that Z/X at the base of the convection zone, $(Z/X)_{\text{conv}}$, should be identical with the value at the photosphere, $(Z/X)_{\text{surf}}$, which is determined spectroscopically.

Table 1 summarizes the microphysics and parameters of the seismic solar models adopted in the present work. We adopt the updated microphysics which was also used by BP98. Table 2 summarizes the differences in some important nuclear cross-section factors between TS98a and this work (Adelberger et al. 1998). As for the helioseismically determined sound-speed profile, we adopt Basu's (1998) results obtained by inversion of the MDI velocity data of the first 144 days. The formal error of the sound-speed inversion is smaller than 0.05% in the region $0.2 \leq r/R_\odot \leq 0.8$, and does not exceed 0.3% in the entire region. In the central core ($r/R_\odot \leq 0.05$), we extrapolate the inverted sound-speed profile and its error level to the center.

3. Structure of the Seismic Solar Model with Homogeneous Z

We first construct a seismic solar model by assuming that Z is homogeneous. The methodology is exactly the same as that adopted by TS98a. The properties of the homogeneous Z model are summarized in table 3.

The effect of various uncertainties in microphysics upon the seismic model and the theoretically expected neutrino fluxes was investigated by a Monte Carlo simulation. For example, as for each of the nuclear cross sections, we constructed one hundred sets of seismic models by superimposing Gaussian noise corresponding to the $1\text{-}\sigma$ level uncertainty of each one of the astrophysical S -factors, while keeping other microphysics unchanged so as to isolate the effect of each microphysics. As for the inverted sound-speed profile, we also constructed one hundred sets of seismic solar models by adding Gaussian noise to the most likely sound-speed at every step of $\Delta r/R_\odot = 0.01$. In this process, we interpolated the sound-speed at the other mesh points smoothly. We estimated the effect of the uncertainties in opacity by constructing an additional

one hundred sets of seismic models with opacities having Gaussian noise with 5% amplitude added in the whole range of density, temperature and chemical compositions at all mesh points. To see the effect of the equation of state, we constructed a seismic solar model with the ideal gas law, and compared the model structure with that constructed with the OPAL equation of state. Table 4 summarizes the effect of the uncertainties in microphysics, investigated in this way, upon the theoretically expected neutrino fluxes, the central density, ρ_c , and the helium abundance at the surface and the base of the convection zone, Y_{conv} , of the seismic solar model.

It is clear from this table that the influences of the $S(0)$ -factors of ${}^1\text{H}(p, e^+ \nu_e){}^2\text{H}$ -, ${}^3\text{He}({}^4\text{He}, \gamma){}^7\text{Be}$ -, and ${}^7\text{Be}(p, \gamma){}^8\text{B}$ -reactions are crucial for the neutrino fluxes. The increase in the $S_{11}(0)$ -factor makes the nuclear energy generation more efficient. Since the luminosity should be fixed, this means that the temperature and density near the center should become lower. Since the sound-speed ($c^2 = \Gamma_1 P / \rho \approx \Gamma_1 RT / \mu$) is also fixed, the decrease in the temperature, T_c , and in the density, ρ_c , leads to an increase in the hydrogen abundance, X_c , and a decrease in the pressure, P_c , respectively. Decreases in ρ_c and T_c make the pp-II and the pp-III reactions less efficient. Thus, the ${}^7\text{Be}$ - and the ${}^8\text{B}$ -neutrino fluxes decrease and, hence, the neutrino capture rates for both the chlorine experiment and Super-Kamiokande become smaller. The decrease in the ${}^7\text{Be}$ - and the ${}^8\text{B}$ -neutrino fluxes dominates over a slight increase in the pp-neutrino flux; the neutrino capture rate for the gallium experiments also decrease. The increase in the $S_{33}(0)$ -factor makes the pp-I reaction more efficient, and thus the contributions of the pp-II- and pp-III reactions to the energy generation become smaller. Hence, the ${}^7\text{Be}$ - and the ${}^8\text{B}$ -neutrino fluxes caused by the pp-II and the pp-III reactions, respectively, decrease, and then the neutrino capture rates for the chlorine experiment and the Super-Kamiokande decrease. Decreases in the ${}^7\text{Be}$ - and the ${}^8\text{B}$ -neutrino fluxes also lead to a decrease in the neutrino capture rate for the gallium experiments. On the other hand, an increase in the $S_{34}(0)$ -factor makes the branching ratio of the pp-II and pp-III reaction to the pp-I reaction larger. Consequently, the ${}^7\text{Be}$ - and the ${}^8\text{B}$ -neutrino fluxes increase, and the neutrino capture rates for all of the neutrino detection experiments increase. The increase in the $S_{17}(0)$ -factor makes the branching ratio of the pp-III reaction to the pp-II reaction larger. Hence it makes the ${}^8\text{B}$ -neutrino flux and the neutrino capture rates for the chlorine experiment and the Super-Kamiokande particularly larger. For the neutrino capture rate for the gallium experiments, the uncertainty in the neutrino cross-section is also crucial because the uncertainty is larger than that for the chlorine detector. On the other hand, the mass ratio of metal to hydrogen at the surface, $(Z/X)_{\text{surf}}$, the depth of the convection zone, r_{conv}/R_\odot , the opacity, and the equation of state are crucial for the surface helium abundance, Y_{conv} . Among them, $(Z/X)_{\text{surf}}$ is crucial because it is related to Y_{conv} directly and its uncertainty is large.

A comparison of the present result with observations

and some other solar models are summarized in table 5 and depicted in figure 2. Note that errors of TS98a and TS98b are rough estimations. The seismic solar model presented by TS98a was constructed with the same assumption of Z as in the present case. We thus regard the present model as a revised version of TS98a. While the sound-speed profile is replaced with the updated one, the difference is so small that this replacement does not induce a significant difference in the structure of the model. Rather, the difference in the model structure comes mainly from the updated input microphysics. As can be seen in table 5, the neutrino-capture rates actually detected in the current experiments are still significantly less than predictions based on the present seismic solar model.

Figure 3 shows the relative differences in the sound-speed profile and in the density profile between the present seismic solar model and a direct inversion of the oscillation data (Basu 1998). For a comparison, the differences between the standard evolutionary model (BP98) and the direct inversion are also shown. Since we imposed a constraint of the inverted sound-speed profile in constructing the seismic solar model, the relative difference in the sound-speed of the seismic model shown in the left panel is exactly equal to the amount of the uncertainty in the inverted sound-speed profile, itself. Note that the difference between the sound-speed profile of the evolutionary standard model (e.g., BP98) and the helioseismically inverted profile is larger than the $1\text{-}\sigma$ level of uncertainty. The seismic model is consistent with the inverted density profile only within the $2\text{-}\sigma$ level, while the difference between the density profile of the evolutionary standard model (BP98) and the inverted profile is larger than the $2\text{-}\sigma$ level near the base of the convective zone.

The uncertainty in the density profile of the seismic solar model is, however, larger than the $1\text{-}\sigma$ level uncertainty of the inverted result. Note that the origin of each uncertainty is different. The uncertainty of the inverted result is caused by the measurement errors of solar oscillations. In order to see what is the main cause of the large uncertainty of the seismic solar model, we carried out a Monte Carlo simulation while changing only one input microphysics, and keeping all others unchanged to isolate the effect of each microphysics. Figure 4 shows the uncertainty in the density profile, caused only by each input microphysics. The influence of the highly accurate sound-speed profile is very small. From this simulation, it is concluded that the main causes are the nuclear cross-sections of the pp-reaction [$S_{11}(0)$] and of the ${}^3\text{He}+{}^4\text{He}$ -reaction [$S_{34}(0)$]. Since energy generation in the Sun is mainly controlled by $S_{11}(0)$, it is most crucial for the solar structure: density profile. Although $S_{34}(0)$ is less important than $S_{11}(0)$ for the solar structure, its uncertainty is much larger.

Figure 3b shows that the uncertainty in the density profile of the seismic model is very small around $r = 0.2R_{\odot}$. Since the total luminosity is fixed, with the increase of $S_{11}(0)$, which is most important for the density profile, the density in the core decreases to compensate for the increase in the nuclear reaction rate. On the other hand,

since the total mass is fixed, the density outside the core increases to compensate for the decrease of the density in the core. Because these opposite reactions of the density against the input physical parameter balance around $r = 0.2R_{\odot}$, the uncertainty in the density of the seismic model is very small around there.

4. Structure of the Seismic Solar Model with a Low- Z Core

Solar models having a low- Z core are expected to lead to low neutrino fluxes. One possible scenario for the formation of a low- Z core is to assume that dust and heavy elements remaining in the disk around the Sun after the formation of the planets were accreted onto the Sun so that heavy elements would be accumulated more in the envelope than in the core (Joss 1974; Jeffery et al. 1997). In another unconventional scenario, heavy elements locked up in grains are assumed to be segregated from the hydrogen and helium gas in the pre-solar nebula (Levy, Ruzmaikina 1994). In order to see how much the neutrino fluxes can be reduced by introducing a low- Z core, we constructed seismic solar models having a low- Z core with the imposition of the sound-speed profile. We assume here that the Z -profile is a step function of r ; that is, $Z(r)$ is a certain constant, Z_c , in the region $0 \leq r \leq r_f$, where r_f is a parameter, while Z is another constant in the region $r_f \leq r \leq r_{\text{conv}}$, so that Z/X matches its surface value, $(Z/X)_{\text{surf}}$ (figure 1 b). The parameter Z_c ranges from 0.0001 to 0.020. We constructed the models so that their sound-speed profiles would be consistent with the seismically determined profile. Table 6 shows the properties of low- Z core models with various values of r_f in the case of $Z_c = 0.0001$. Note that the model with $r_f = 0$ is the same as the homogeneous Z model discussed in the previous section. In this table, M_{core} denotes the mass of the low- Z core [$M_{\text{core}} \equiv M_r(r = r_f)$].

The properties of the low- Z core models can be explained as follows. With an increase in the low- Z core size, the opacity in the core decreases, resulting in a decrease of the central temperature. Since the sound-speed profile is fixed by the observation, this requires a decrease in the mean molecular weight to compensate for a decrease in the temperature, and hence an increase in the hydrogen abundance there. The total luminosity is also fixed, which requires an increase in the density in the core to compensate for the decrease in the nuclear reaction rate due to the decrease in temperature there [cf. equation (3)]. The constraint of the sound-speed leads to an increase in the pressure in the core because of the higher density. These tendencies are common in the seismic solar models with a low- Z core, and become conspicuous with a decrease in the value of Z_c .

Figures 5 a-c show the dependence of the neutrino capture rates of the seismic models upon the values of Z_c and M_{core} . For a comparison, the detected neutrino capture rates are also indicated. The neutrino capture rates for the chlorine detector (Homestake) and the ${}^8\text{B}$ -neutrino flux (Super-Kamiokande) decrease substantially with an

increase in the low- Z core size.

The effect of various uncertainties in microphysics upon the model properties and the theoretically expected neutrino fluxes was investigated by a Monte Carlo simulation in the same way as that described in the previous section. The results are summarized in table 7 for the case of $Z_c = 0.0001$; also, the thus-determined error bars for the neutrino capture rates, the ^8B -neutrino flux and the central density are depicted in figure 5.

Let us focus attention on those models with $Z_c = 0.0001$ (the continuous line). As can be seen in figure 5 a, the models with $M_{\text{core}} > 0.1M_\odot$ do not contradict the result of the Homestake experiment if we tolerate the difference within the $2\text{-}\sigma$ level. In the same sense, the Super-Kamiokande experiment is consistent with those models having $0.05M_\odot \leq M_{\text{core}} \leq 0.12M_\odot$. That is, low- Z core models with $M_{\text{core}} \sim 0.1M_\odot$ are favorable for explaining the Homestake and the Super-Kamiokande experiments simultaneously. Besides that, such models are naturally consistent with the seismically determined sound-speed profile. These results are not in agreement with the conclusion of Guenther and Demarque (1997, hereafter we refer to it as GD97), who investigated the low- Z core model of the Sun by following its evolution. There are differences between the present approach and GD97's in the concept and methodology of making solar models. While the models of GD97 are constructed following the stellar evolution, the present models are not. In this sense the present approach has more freedom. We do not try to explain how our seismic models can be realized in the evolutionary process, and such an investigation is beyond our scope. While the present models were constructed with fine tuning to agree with the helioseismic data, those of GD97 were not. It also should be noted that GD97 adopted almost the same input physical parameters with TS98a. Updating them in GD97's approach may lead to lower neutrino fluxes (cf. figure 2 and table 5), and the difference between the present result and GD97's would become smaller. Our results demonstrate that certain low- Z core models of the Sun can be in agreement with the Homestake and the Super-Kamiokande data and helioseismology. Therefore, criticisms based on evolutionary models are not necessarily fair. However, even the present seismic solar models are substantially in disagreement with the neutrino capture rates for the gallium detectors, GALLEX and SAGE.

In the present approach, we did not use the seismically obtained density profile as a constraint in making seismic solar models. We should compare the density profile of the models with the seismically inverted profile. In the case of $Z_c = 0.0001$, as shown in figure 5 d, the central density of the model becomes higher with an increase in the core size, and only those models with $M_{\text{core}} < 0.02M_\odot$ are consistent with the seismically inverted density (Basu 1998). To see the effect of parameter Z_c , we adopted various values of Z_c and constructed seismic models of the Sun with a low- Z core in a similar way. However, no model is consistent with all of the neutrino experiments and the inverted density profile. From these results, we conclude

that none of the low- Z core models are simultaneously consistent with all of the neutrino experiments and the helioseismically inverted density profile.

In the case of $Z_c > Z_{\text{surf}} (\approx 0.018)$, the temperature at the central region becomes higher than that of the homogeneous Z model, and hence deviations from the detected solar neutrino fluxes become larger, while the density at the central region becomes less inconsistent with the seismically inverted profile.

5. Summary and Conclusion

We have revised the seismic solar model with a constraint of the sound-speed profile, and the latest input microphysics and physical parameters, assuming that Z is uniform, and also have estimated the uncertainty of the seismic model thoroughly by a Monte Carlo simulation. Though the seismic solar model thus constructed is naturally consistent with the helioseismic data, the expected neutrino fluxes based on this model are still higher than the experimental data. This result implies that a modification of the solar model does not seem to be able to solve the solar neutrino problem, leaving the neutrino-oscillation explanation as an attractive possibility. The uncertainty in the seismically determined sound-speed profile is so small that it does not induce substantial uncertainties in the physical properties of the model. The uncertainties in the nuclear cross-section [especially $S_{11}(0)$, $S_{34}(0)$, and $S_{17}(0)$] have more crucial influences.

We have also constructed seismic models with an assumption of a low- Z core, and evaluated the neutrino fluxes of these models to see if these nonstandard solar models can solve the solar neutrino problem. Although it turns out to be possible to explain the neutrino fluxes for both the Homestake and Super-Kamiokande experiments and the sound-speed profile simultaneously by the low- Z core extending $\sim 0.01M_{\text{core}}/M_\odot$, it is still impossible to explain all of the data, including the neutrino flux measurements based on the gallium detectors, by this model. The density in the core becomes higher with a decrease of Z_c , and the model becomes less consistent with a seismically inverted density profile.

Therefore, we conclude that the low- Z core models of the Sun cannot explain all of the solar neutrino detection experiments and the helioseismically inverted sound-speed and density profiles.

We would like to thank M. Takata for many useful discussions. One of the authors (SW) would like to express his sincere thanks to Professor H. Saio for guidance, continuous encouragement and many useful discussions during his fruitful campus life in Tohoku University. This research was supported in part by a Grant-in-Aid for Scientific Research on Priority Areas by the Ministry of Education, Culture, Sports, Science and Technology (12047208).

References

- [Abdurashitov et al.(1999)] Abdurashitov, J.N., Gavrin, V.N., Girin, S.V., Gorbachev, V.V., Ibragimova, T.V., Kalikhov, A.V., Khairnasov, N.G., Knodel, T.V., et al. 1999, *Phys. Rev. C*, 60, 055801
- [Adelberger(1998)] Adelberger, E.G., Austin, S.M., Bahcall, J.N., Balantekin, A.B., Bogaert, G., Brown, L.S., Buchmann, L., Cecil, F.E., et al. 1998, *Rev. Mod. Phys.*, 70, 1265
- [Bahcall(1997)] Bahcall, J.N. 1997, *Phys. Rev. C*, 56, 3391
- [Bahcall et al.(1998)] Bahcall, J.N., Basu, S., & Pinsonneault, M.H. 1998, *Phys. Lett. B*, 433, 1 (BP98)
- [Bahcall et al.(1996)] Bahcall, J.N., Lisi, E., Alburger, D.E., de Braeckeleer, L., Freedman, S.J., & Napolitano, J. 1996, *Phys. Rev. C*, 54, 411
- [Bahcall et al.(1995)] Bahcall, J.N., Pinsonneault, M.H., & Wasserburg, G.J. 1995, *Rev. Mod. Phys.*, 67, 781
- [Bahcall et al.(1997)] Bahcall, J.N., Pinsonneault, M.H., Basu, S., & Christensen-Dalsgaard, J. 1997, *Phys. Rev. Lett.*, 78, 171
- [Basu(1998)] Basu, S. 1998, *MNRAS*, 298, 719
- [Basu, Antia(1997)] Basu, S., & Antia, H.M. 1997, *MNRAS*, 287, 189
- [Cleveland et al.(1998)] Cleveland, B.T., Daily, T., Davis, R., Jr., Distel, J.R., Lande, K., Lee, C.K., Wildenhain, P.S., & Ullman, J. 1998, *ApJ*, 496, 505
- [Fukuda et al.(1998)] Fukuda, Y., Hayakawa, T., Ichihara, E., Inoue, K., Ishihara, K., Ishino, H., Itow, Y., Kajita, T., et al. 1998, *Phys. Rev. Lett.*, 81, 1158
- [Fukuda et al.(1996)] Fukuda, Y., Hayakawa, T., Inoue, K., Ishihara, K., Ishino, H., Joukou, S., Kajita, T., Kasuga, S., et al. 1996, *Phys. Rev. Lett.*, 77, 1683
- [García et al.(1991)] García, A., Adelberger, E.G., Magnus, P.V., Swanson, H.E., Tengblad, O., & ISOLDE Collaboration 1991, *Phys. Rev. Lett.*, 67, 3654
- [Gough(1984)] Gough, D.O. 1984, *Phil. Trans. R. Soc. London, A*, 313, 27
- [Gough(1999)] Gough, D.O. 1999, *Nuc. Phys. B*, 77, 81
- [Grevesse, Noels(1993)] Grevesse, N., & Noels, A. 1993, in *Origin and Evolution of the Elements*, ed. N. Prantzos, E. Vangioni-Flam, & M. Cassé (Cambridge: Cambridge University Press), p.15
- [Gruzinov, Bahcall(1998)] Gruzinov, A.V., & Bahcall, J.N. 1998, *ApJ*, 504, 996
- [Guenther, Demarque(1997)] Guenther, D.B., & Demarque, P. 1997, *ApJ*, 484, 937 (GD97)
- [Hampel et al.(1999)] Hampel, W., Handt, J., Heusser, G., Kiko, J., Kirsten, T., Laubenstein, M., Pernicka, E., Rau, W., et al. 1999, *Phys. Lett. B*, 447, 127
- [Iglesias, Rogers(1996)] Iglesias, C.A., & Rogers, F.J. 1996, *ApJ*, 464, 943
- [Jeffery et al.(1997)] Jeffery, C.S., Bailey, M.E., & Chambers, J.E. 1997, *Observatory*, 117, 224
- [Joss(1974)] Joss, P.C. 1974, *ApJ*, 191, 771
- [Levy, Ruzmaikina(1994)] Levy, E.H., & Ruzmaikina, T.V. 1994, *ApJ*, 431, 881
- [Rogers et al.(1996)] Rogers, F.J., Swenson, F.J., & Iglesias, C.A. 1996, *ApJ*, 456, 902
- [Salpeter(1954)] Salpeter, E.E. 1954, *Australian J. Phys.*, 7, 373
- [Shibahashi(1993)] Shibahashi, H. 1993, in *Frontiers of Neutrino Astrophysics*, ed. Y. Suzuki, & K. Nakamura (Tokyo: Universal Academy Press), p.93
- [Shibahashi(1999)] Shibahashi, H. 1999, *Adv. Space Res.*, 24, 137
- [Shibahashi et al.(2000)] Shibahashi, H., Hosogai, M., & Takata, M. 2000, in *Neutrino Oscillations and their Origin*, ed. Y. Suzuki, M. Nakahata, M. Shiozawa, & K. Kaneyuki (Tokyo: Universal Academy Press), p.215
- [Shibahashi, Takata(1996)] Shibahashi, H., & Takata, M. 1996, *PASJ*, 48, 377
- [Takata, Shibahashi(1998)] Takata, M., & Shibahashi, H. 1998a, *ApJ* 504, 1035 (TS98a)
- [Takata, Shibahashi(1998)] Takata, M., & Shibahashi, H. 1998b, in *SOHO 6/GONG 98 Workshop: Structure and Dynamics of the Interior of the Sun and Sun-like Stars*, ed. S. Korzenik, & A. Wilson (Noordwijk: ESA Publication Division), p.543 (TS98b)
- [Takata, Shibahashi(1999)] Takata, M., & Shibahashi, H. 1999, *Adv. Space Res.*, 24, 181
- [Watanabe, Shibahashi(2000)] Watanabe, S., & Shibahashi, H. 2000, in *SOHO-10/GONG-2000 Workshop: Helio- and Asteroseismology at the Dawn of the Millennium*, ed P. Pallé, & A. Wilson (Noordwijk: ESA Publication Division), p.567

Table 1. The Microphysics and physical parameters of the seismic solar models.

Physics/Parameter		Reference
Equation of state	OPAL	Rogers et al. 1996
Opacity	OPAL	Iglesias, Rogers 1996
Nuclear cross-section		Adelberger et al. 1998
Screening effect	Weak screening	Salpeter 1954; Gruzinov, Bahcall 1998
Neutrino cross-section		Bahcall 1997; Bahcall et al. 1996, 1998
		García et al. 1991
$(Z/X)_{\text{surf}}$	0.0245	Grevesse, Noels 1993
Luminosity L_{\odot}	$3.844(1 \pm 0.004) \times 10^{33} \text{erg s}^{-1}$	Bahcall, Pinsonneault 1995
Sound-speed profile	SOHO data	Basu 1998
r_{conv}	$(0.713 \pm 0.001)R_{\odot}$	Basu, Antia 1997

Table 2. Comparison of some important nuclear cross-section factors between TS98a and this work.

Reference	TS98a		This work	
	Bahcall, Pinsonneault 1995		Adelberger et al. 1998	
	$S(0)$ (keV barns)	$S'(0)$ (barns)	$S(0)$ (keV barns)	$S'(0)$ (barns)
${}^1\text{H}(p, e^+ \nu_e){}^2\text{H}$..	$3.89(1 \pm 0.011) \times 10^{-22}$	4.52×10^{-24}	$4.00(1 \pm 0.007^{+0.020}_{-0.011}) \times 10^{-22}$	4.48×10^{-24}
${}^3\text{He}({}^3\text{He}, 2p){}^4\text{He}$	$4.99(1 \pm 0.06) \times 10^3$	-0.9	$(5.4 \pm 0.4) \times 10^3$	-4.1
${}^3\text{He}({}^4\text{He}, \gamma){}^7\text{Be}$.	$0.524(1 \pm 0.032)$	-3.1×10^{-4}	0.53 ± 0.05	-3.0×10^{-4}
${}^7\text{Be}(p, \gamma){}^8\text{B}$	$0.0224(1 \pm 0.093)$	-3×10^{-5}	$0.019^{+0.004}_{-0.002}(1\sigma)^{+0.008}_{-0.004}(3\sigma)$	-1.3×10^{-5}
${}^{14}\text{N}(p, \gamma){}^{15}\text{O}$...	$3.29(1 \pm 0.12)$	-5.91×10^{-3}	$3.5^{+0.4}_{-1.6}(1\sigma)^{+1.0}_{-2.0}(3\sigma)$	-1.28×10^{-2}

Table 3. Properties of the seismic solar model with homogeneous Z .

Quantities	Most likely values
T_c (10^7 K)	$1.561^{+0.005}_{-0.009}$
P_c (10^{17} dyn cm^{-2})	$2.378^{+0.031}_{-0.049}$
ρ_c (g cm^{-3})	$156.0^{+2.0}_{-3.3}$
X_c	$0.3383^{+0.0058}_{-0.0035}$
Y_c	$0.6437^{+0.0035}_{-0.0058}$
$M_{\text{conv}}/M_{\odot}$	$0.0264^{+0.0008}_{-0.0013}$
T_{conv} (10^6 K)	2.19 ± 0.01
P_{conv} (10^{13} dyn cm^{-2})	$5.71^{+0.07}_{-0.06}$
ρ_{conv} (g cm^{-3})	0.190 ± 0.001
X_{conv}	$0.7365^{+0.0036}_{-0.0037}$
Y_{conv}	$0.2455^{+0.0042}_{-0.0041}$
Z_{conv}	0.0180 ± 0.0004
pp ν flux (10^{10} cm^{-2} s^{-1}) .	$5.98^{+0.05}_{-0.04}$
pep ν flux (10^8 cm^{-2} s^{-1}) .	1.44 ± 0.02
hep ν flux (10^3 cm^{-2} s^{-1}) .	2.11 ± 0.06
${}^7\text{Be}$ ν flux (10^9 cm^{-2} s^{-1}) .	$4.72^{+0.39}_{-0.43}$
${}^8\text{B}$ ν flux (10^6 cm^{-2} s^{-1}) ..	$4.77^{+1.04}_{-0.72}$
${}^{13}\text{N}$ ν flux (10^8 cm^{-2} s^{-1}) .	$4.43^{+0.49}_{-1.26}$
${}^{15}\text{O}$ ν flux (10^8 cm^{-2} s^{-1}) .	$4.15^{+0.49}_{-1.26}$
${}^{17}\text{F}$ ν flux (10^6 cm^{-2} s^{-1}) .	$5.22^{+1.08}_{-1.16}$
ν capture rate for Cl (SNU)	$7.17^{+1.24}_{-0.95}$
ν capture rate for Ga (SNU)	$126^{+6.6}_{-5.3}$

Table 4. Sensitivity of the neutrino fluxes, the central density, ρ_c , and the surface helium abundance, Y_{conv} , to the uncertainties in the input physics.*

			Cl	Ga	^8B	ρ_c	Y_{conv}
			7.17	126	4.77	156	0.246
Input physics			(SNU)	(SNU)	($10^6\text{cm}^{-2}\text{s}^{-1}$)	(g cm^{-3})	
pp	$4.00(1^{+0.021}_{-0.013}) \times 10^{-22}$	(keV b)	-0.633	-3.1	-0.477	-3.0	+0.0008
pep	$\pm 1\%$		+0.372	+1.8	+0.282	+1.6	-0.0003
$^3\text{He}^3\text{He}$	5.4 ± 0.32	(MeV b)	∓ 0.131	∓ 0.8	∓ 0.094	± 0.3	∓ 0.0001
$^3\text{He}^4\text{He}$	0.53 ± 0.05	(keV b)	± 0.408	± 2.6	± 0.293	∓ 1.0	± 0.0003
$^7\text{Be}+e$	$\pm 2\% (1\sigma)$		∓ 0.106	∓ 0.2	∓ 0.093	0.0	0.0000
$^7\text{Be}+p$	$19^{+4}_{-2}(1\sigma)^{+8}_{-4}(3\sigma)$	(eV b)	+1.057	+2.2	+0.927	0.0	0.0000
$^{12}\text{C}+p$	1.34 ± 0.21	(keV b)	-0.456	-1.0	-0.400	0.0	0.0000
$^{13}\text{C}+p$	7.6 ± 1	(keV b)	0.000	0.0	0.000	0.0	0.0000
$^{14}\text{N}+p$	$3.5^{+0.4}_{-1.6}(1\sigma)^{+1.0}_{-2.0}(3\sigma)$	(keV b)	+0.023	+0.5	-0.007	-0.2	+0.0001
$^{16}\text{O}+p$	9.4 ± 1.7	(keV b)	-0.069	-1.6	+0.021	+0.6	-0.0002
$(Z/X)_{\text{surf}}$	0.0245 ± 0.0006		± 0.120	± 0.5	± 0.094	∓ 0.2	± 0.0026
L_{\odot}	$3.844(1 \pm 0.004) \times 10^{33}$	(erg s $^{-1}$)	± 0.203	± 1.3	± 0.153	± 0.5	± 0.0005
Sound-speed profile			± 0.030	± 0.1	± 0.022	± 0.3	± 0.0001
$r_{\text{conv}}/R_{\odot}$	0.713 ± 0.001		∓ 0.031	∓ 0.2	∓ 0.023	0.0	± 0.0031
Neutrino cross-section			± 0.173	$^{+5.1}_{-2.4}$
Opacity	$\pm 5\%$		(\pm)0.083	(\pm)0.4	(\pm)0.062	(\pm)0.2	(\pm)0.0075
EOS	ideal ($\Gamma = \frac{5}{3}$)		-0.007	-0.3	+0.006	-0.6	+0.012
Total	$\sqrt{\sigma^2 + \sigma^2 + \dots}$		+1.24	+6.6	+1.04	+2.0	± 0.004
(except for opacity and EOS)			-0.95	-5.3	-0.72	-3.2	

* The first ten entries are due to the nuclear cross-section factors. References for each uncertainty are the same as given in table 1 except for $(Z/X)_{\text{surf}}$. The uncertainty of $(Z/X)_{\text{surf}}$ is taken from Basu (1998).**Table 5.** Comparison of experiments and some solar models.

	Experiments	This work	TS98a	TS98b	BP98
Cl(SNU)	2.56 ± 0.23 *	$7.17^{+1.24}_{-0.95}$	$7.8 \sim 10.6$	$7.7 \sim 8.8$	$7.7^{+1.2}_{-1.0}$
Ga(SNU)	$67.2^{+8.0}_{-7.6}$ † $77.5^{+7.5}_{-7.8}$ ‡	$126^{+6.6}_{-5.3}$	$129 \sim 142$	$132 \sim 138$	129^{+8}_{-6}
$^8\text{B}(10^6 \text{cm}^{-2} \text{s}^{-1})$	2.80 ± 0.38 § $2.42^{+0.12}_{-0.09}$	$4.77^{+1.04}_{-0.72}$	$5.48 \sim 7.67$	$5.3 \sim 6.1$	$5.15^{+0.98}_{-0.72}$
$\rho_c(\text{g cm}^{-3})$	153.9 ± 1.1 ‡	$156^{+2.0}_{-3.2}$	$156 \sim 171$	$153 \sim 155$	~ 152.2
Y_{conv}	0.248 ± 0.001 ‡	0.246 ± 0.004	$0.227 \sim 0.236$	$0.246 \sim 0.247$	~ 0.243

* Homestake : Cleveland et al. 1998

† SAGE : Abdurashitov et al. 1999

‡ GALLEX : Hampel et al. 1999

§ Kamiokande : Fukuda et al. 1996

|| Super-Kamiokande : Fukuda et al. 1998

‡ Basu 1998

Table 6. Properties of the low- Z core model in the case of $Z_c = 0.0001$.*

r_f/R_\odot	0.000	0.050	0.069	0.083	0.10	0.12	0.13	0.15
M_{core}/M_\odot	0.000	0.013	0.030	0.050	0.080	0.117	0.150	0.202
$T_c(10^7 \text{ K})$	1.56	1.53	1.51	1.49	1.48	1.46	1.46	1.45
$P_c(10^{17} \text{ dyn cm}^{-2})$..	2.38	2.40	2.41	2.43	2.44	2.46	2.48	2.50
$\rho_c(\text{g cm}^{-3})$	156	157	158	159	160	162	163	164
X_c	0.338	0.356	0.369	0.378	0.387	0.395	0.399	0.403
Y_c	0.644	0.644	0.631	0.622	0.613	0.605	0.601	0.597
$T_{\text{conv}}(10^6 \text{ K})$	2.20	2.19	2.19	2.20	2.20	2.19	2.19	2.19
$P_{\text{conv}}(10^{13} \text{ dyn cm}^{-2})$	5.71	5.70	5.70	5.69	5.68	5.68	5.67	5.66
$\rho_{\text{conv}}(\text{g cm}^{-3})$	0.190	0.190	0.190	0.189	0.189	0.189	0.189	0.189
X_{conv}	0.736	0.737	0.737	0.736	0.737	0.737	0.737	0.738
Y_{conv}	0.246	0.245	0.245	0.246	0.245	0.245	0.245	0.244
Z_{conv}	0.0180	0.0180	0.0180	0.0181	0.0181	0.0181	0.0181	0.0181
Cl(SNU)	7.17	6.50	5.57	4.76	3.84	3.15	2.78	2.45
Ga(SNU)	126	122	117	114	109	105	103	101
$^8\text{B}(10^6 \text{ cm}^{-2} \text{ s}^{-1})$	4.77	4.33	3.63	3.00	2.30	1.79	1.52	1.29

* The first two rows indicate the radius fraction and the mass fraction of the low- Z core, respectively.

Table 7. Sensitivity of the neutrino fluxes and the central density, ρ_c , of the low- Z core model with $Z_c = 0.0001$ and $r_f/R_\odot = 0.12$ ($M_{\text{core}}/M_\odot = 0.117$) to the uncertainties in the input physics.*

Input physics			Cl	Ga	^8B	ρ_c
			3.15 (SNU)	105 (SNU)	1.79 ($10^6 \text{ cm}^{-2} \text{ s}^{-1}$)	162 (g cm^{-3})
pp	$4.00(1^{+0.021}_{-0.013}) \times 10^{-22}$	(keV b)	-0.249 $+0.141$	-1.5 $+0.8$	-0.179 $+0.103$	-3.4 $+1.8$
pep	$\pm 1\%$		± 0.002	0.0	0.000	0.0
$^3\text{He}^3\text{He}$	5.4 ± 0.32	(MeV b)	∓ 0.066	∓ 0.6	∓ 0.040	± 0.3
$^3\text{He}^4\text{He}$	0.53 ± 0.05	(keV b)	± 0.207	± 1.9	± 0.125	∓ 0.8
$^7\text{Be}+e$	$\pm 2\% (1\sigma)$		∓ 0.040	∓ 0.1	∓ 0.035	0.0
$^7\text{Be}+p$	$19^{+4}_{-2}(1\sigma)^{+8}_{-4}(3\sigma)$	(eV b)	$+0.369$ -0.171	$+0.8$ -0.4	$+0.347$ -0.150	0.0
$^{12}\text{C}+p$	1.34 ± 0.21	(keV b)	0.000	0.0	0.000	0.0
$^{13}\text{C}+p$	7.6 ± 1	(keV b)	0.000	0.0	0.000	0.0
$^{14}\text{N}+p$	$3.5^{+0.4}_{-1.6}(1\sigma)^{+1.0}_{-2.0}(3\sigma)$	(keV b)	$+0.000$ -0.001	0.0	-0.000 $+0.001$	0.0
$^{16}\text{O}+p$	9.4 ± 1.7	(keV b)	0.000	0.0	0.000	0.0
$(Z/X)_{\text{surf}}$	0.0245 ± 0.0006		± 0.024	± 0.2	± 0.017	∓ 0.2
L_\odot	$3.844(1 \pm 0.004) \times 10^{33}$	(erg s^{-1})	± 0.082	± 0.8	± 0.059	± 0.6
Sound-speed profile			± 0.011	± 0.1	± 0.008	± 0.3
r_{conv}/R_\odot	0.713 ± 0.001		∓ 0.005	∓ 0.1	∓ 0.003	± 0.1
Neutrino cross-section			± 0.066	$+3.1$ -1.7
Opacity	$\pm 5\%$		$(\pm)0.025$	$(\pm)0.2$	$(\pm)0.018$	$(\pm)0.1$
EOS	ideal ($\Gamma = \frac{5}{3}$)		+0.001	-0.2	+0.006	-1.1
Total	$\sqrt{\sigma^2 + \sigma^2 + \dots}$		$+0.49$ -0.39	$+4.0$ -3.2	$+0.39$ -0.28	$+2.1$ -3.6
(except for opacity and EOS)			(SNU)	(SNU)	($10^6 \text{ cm}^{-2} \text{ s}^{-1}$)	(g cm^{-3})

* The first ten entries are due to the nuclear cross-section factors. The references for each uncertainty are the same as shown in table 4.

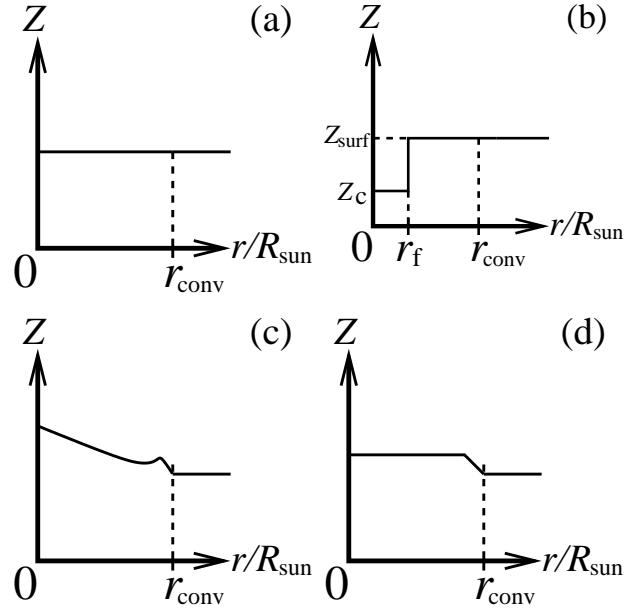


Fig. 1. Comparison of Z distributions. (a) Homogeneous case (section 3, TS98a). (b) Low- Z core (section 4). (c) Evolutionary model with gravitational settling (e.g., BP98). (d) Rectilinear profile (TS98b).

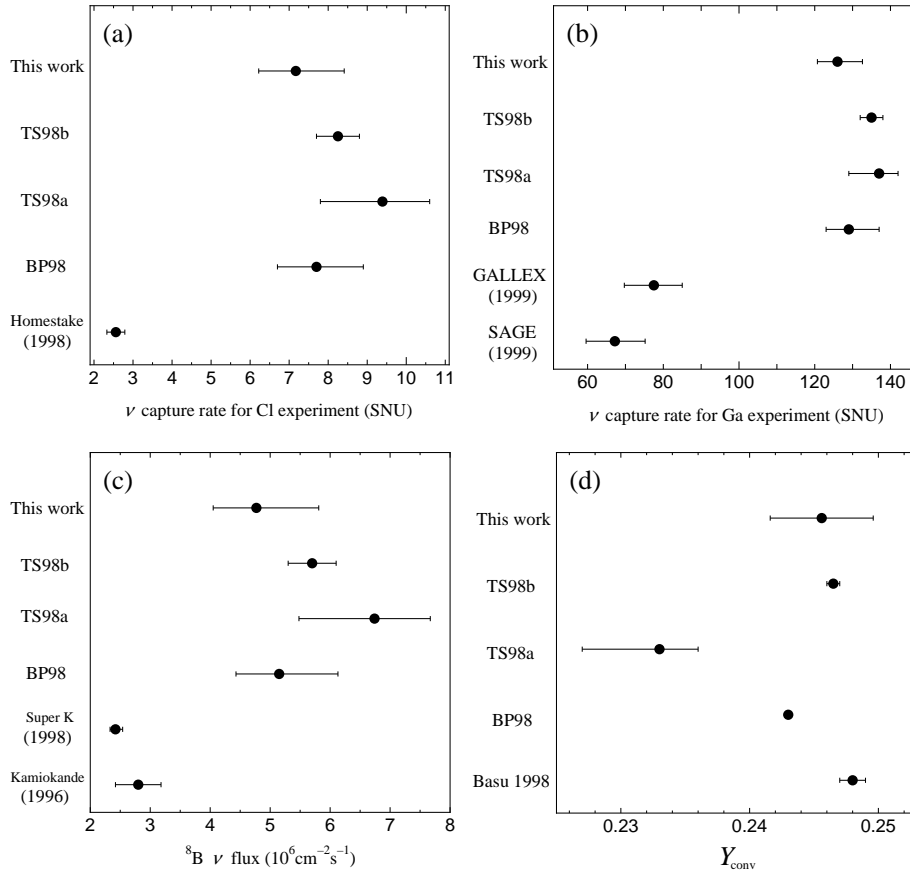


Fig. 2. Comparison of experiments and some solar models. We should regard the errors of TS98a and TS98b as rough estimations. (a) Neutrino capture rate for the chlorine detector at Homestake. (b) Neutrino capture rate for the gallium detectors (GALLEX and SAGE). (c) ^8B -neutrino flux for the Kamiokande and the Super-Kamiokande. (d) Helium abundance at the base of the convection zone and the surface Y_{conv} . For a comparison, the seismically inverted abundance, Y_{conv} (Basu 1998), is also shown.

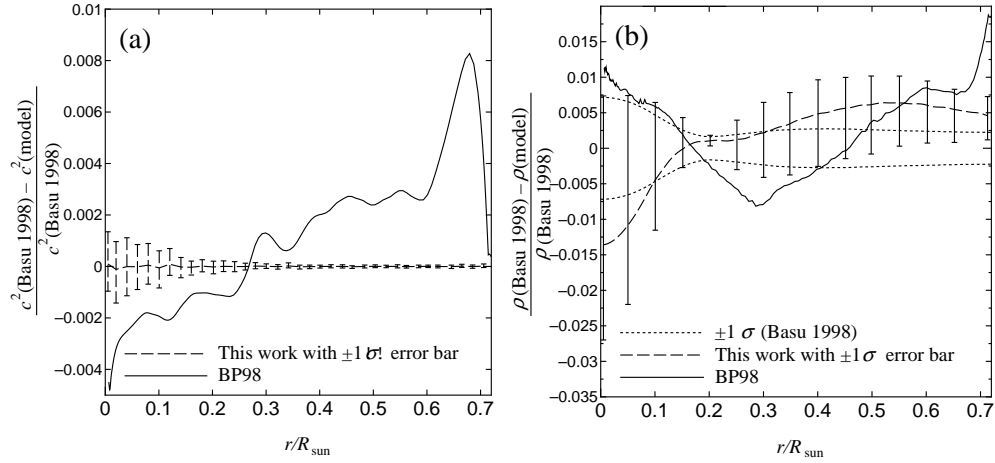


Fig. 3. Relative differences in the squared sound-speed (a) and in the density (b) between the solar models and the seismically determined profiles (Basu 1998). For a comparison, the profiles of an evolutionary solar model (BP98) are also shown.

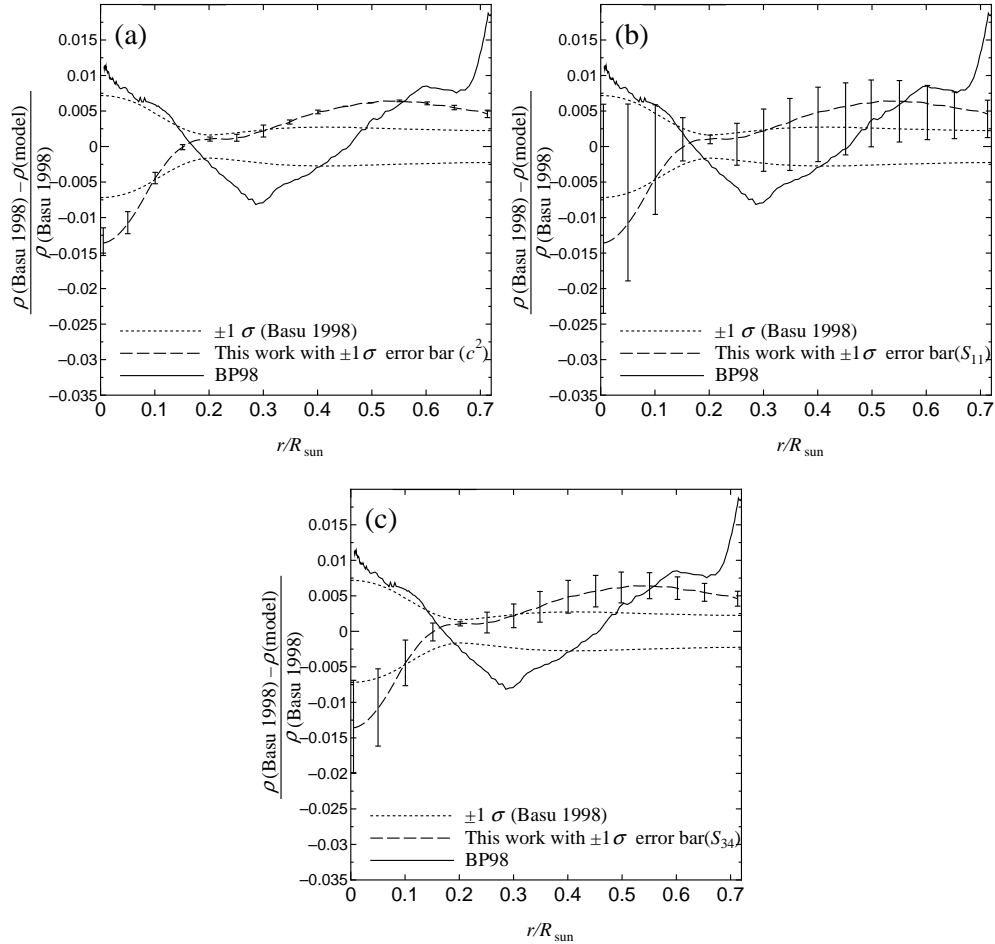


Fig. 4. Uncertainties in the density profile caused only by errors in the sound-speed profile (a), by uncertainties in the nuclear cross-section $S_{11}(0)$ (b), and $S_{34}(0)$ (c).

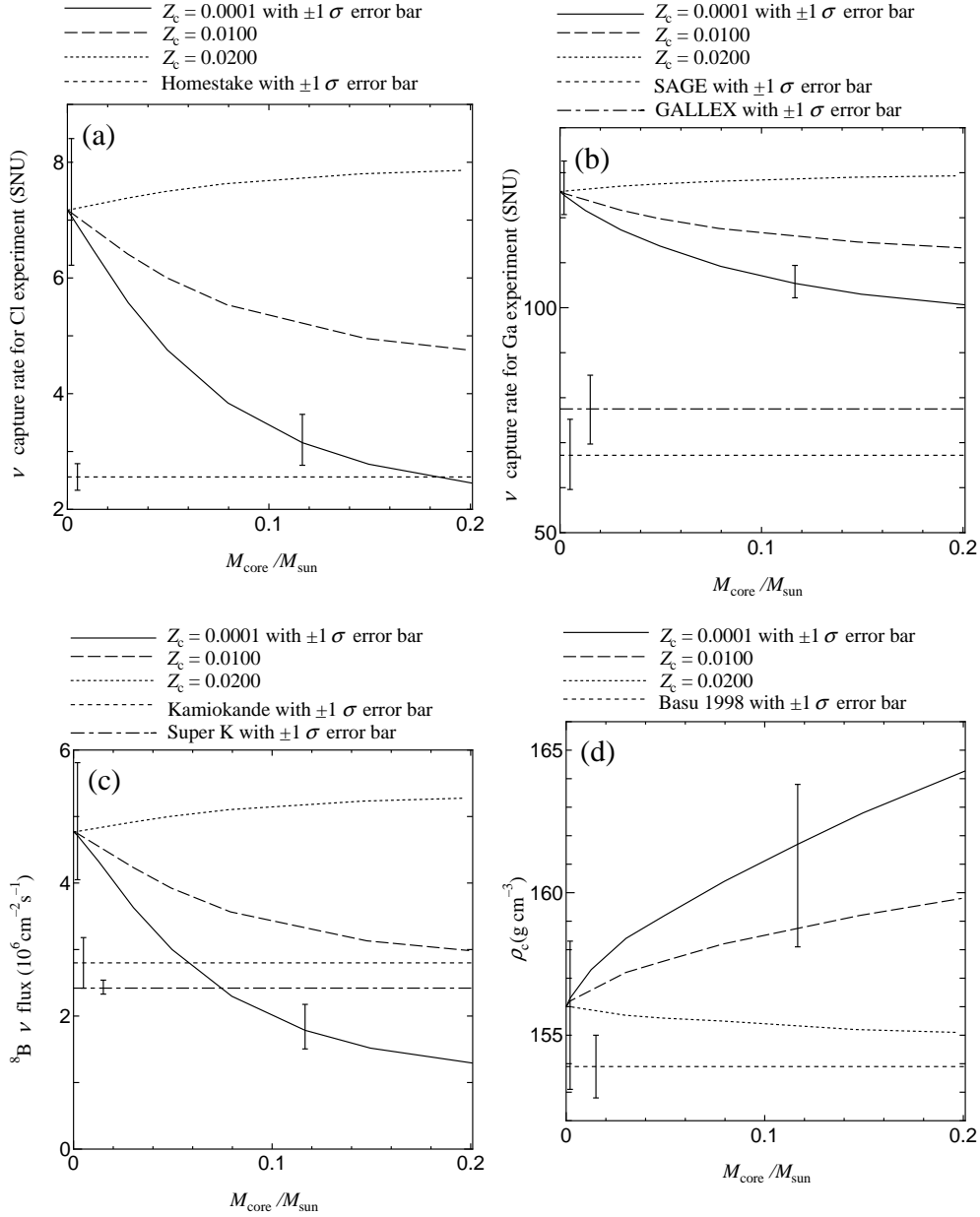


Fig. 5. Dependence of the neutrino fluxes and the central density upon Z_c and the core size. (a) Neutrino capture rate for the chlorine detector at Homestake. (b) Neutrino capture rate for the gallium detectors (GALLEX and SAGE). (c) ^8B -neutrino flux for the Kamiokande and the Super-Kamiokande. (d) Central density. For a comparison, the seismically inverted density, ρ_{obs} (Basu 1998), is also shown with the observational error.